Optical Engineering

OpticalEngineering.SPIEDigitalLibrary.org

Highly birefringent honeycomb cladding terahertz fiber for polarization-maintaining applications

Mohammad Rakibul Islam
Md. Faiyaz Kabir
Khandoker Md. Abu Talha
Md. Shamsul Arefin

SPIE.

Mohammad Rakibul Islam, Md. Faiyaz Kabir, Khandoker Md. Abu Talha, Md. Shamsul Arefin, "Highly birefringent honeycomb cladding terahertz fiber for polarization-maintaining applications," *Opt. Eng.* **59**(1), 016113 (2020), doi: 10.1117/1.OE.59.1.016113

Highly birefringent honeycomb cladding terahertz fiber for polarization-maintaining applications

Mohammad Rakibul Islam,[a,*] Md. Faiyaz Kabir,[a] Khandoker Md. Abu Talha,[a] and Md. Shamsul Arefin[b]

[a]Islamic University of Technology, Department of Electrical and Electronic Engineering, Gazipur, Bangladesh

[b]Green University of Bangladesh, Department of Electrical and Electronic Engineering, Dhaka, Bangladesh

Abstract. A novel Zeonex-based photonic crystal fiber (PCF) with a honeycomb-like cladding structure and a hexagonal slotted core is proposed. The finite-element method is used to numerically analyze the guiding characteristics of the proposed fiber. The investigations are carried out by optimizing various geometrical parameters of the fiber and varying the frequency, core diameter, and core porosity. The results indicate that the designed PCF demonstrates an ultrahigh birefringence of 0.083, extremely low confinement and effective material loss of 10^{-8} and 0.095 cm^{-1}, respectively, and a very high core power fraction of 52.2% at an operating frequency of 1.5 THz. In addition, other guiding properties such as numerical aperture, dispersion, and effective area are also analyzed and discussed in detail. The obtained results show that the proposed PCF is extremely suitable for use in numerous low-loss, polarization-maintaining applications in the terahertz frequency range. © *2020 Society of Photo-Optical Instrumentation Engineers (SPIE)* [DOI: 10.1117/1.OE.59.1.016113]

Keywords: photonic crystal fiber; birefringence; effective material loss; finite-element method.

Paper 190941 received Jul. 11, 2019; accepted for publication Dec. 30, 2019; published online Jan. 21, 2020.

1 Introduction

In recent years, there has been a massive surge in interest regarding applications in the terahertz (THz) frequency range, which extends from 0.1 to 10 THz and lies between the microwave and infrared frequency bands. The THz band provides a number of advantages for a wide variety of applications ranging from biotechnology,[1] security screening,[2] biomedical imaging,[3] optical communication,[4] sensing,[5–8] and noninvasive medical procedures such as the detection of skin cancer.[9] However, in order to utilize THz radiation effectively, it is necessary to guide THz waves in a manner that is suitable for long-distance transmission with minimal wavelength-dependent losses and near-flat dispersion at the desired wavelength. Conventional THz systems that rely on free-space propagation do not fulfill these criteria, namely due to high atmospheric losses and improper reception of THz waves due to the misalignment of transmitter and receiver.

Numerous types of THz waveguides have been proposed in recent years for efficient and reliable THz signal transmission, such as metallic waveguides and bare metal wires,[10] dielectric metal-coated tubes,[11] plastic fibers,[12] polymer tubes,[13,14] and Bragg fiber.[15] However, all of them suffer from very high losses. Metallic waveguides suffer from high bending and attenuation losses and undesirable interaction with complex environments, whereas dielectric waveguides suffer from high material absorption loss due to the dielectric material. Polymer tubes, while having high birefringence, suffer from high atmospheric losses. Recently, a new type of optical fiber called photonic crystal fiber (PCF) has been given a great deal of attention due to its beneficial properties such as high birefringence, low material and confinement losses, low dispersion, and flexibility in modifying the guiding properties by controlling geometrical parameters. Conventional solid core PCFs have high absorption losses.[16] In order to mitigate that, a

*Address all correspondence to Mohammad Rakibul Islam, E-mail: rakibultowhid@yahoo.com

number of microstructured air holes are placed inside the solid core, to form a porous-core PCF. Since dry air does not absorb THz waves, it is essentially a considered a lossless medium for THz transmission.[17] As a result, porous-core PCFs can guide THz waves with much lower effective material loss (EML)[18] by confining most of the mode power inside the air holes.

In addition to low absorption loss, modal birefringence is one of the most important properties of a PCF. Birefringence is defined as the absolute difference of the refractive indices of the x and y polarization modes. Typically, birefringence is induced in a porous-core PCF by breaking the symmetric characteristics of the core or cladding,[19] causing the light to separate into two polarized components. High birefringence allows a PCF to maintain polarization characteristics for long-distance THz transmission. This is crucial for many polarization-sensitive applications such as time-domain spectroscopy,[20,21] optical sensing,[22] and polarized filtering of THz waves.[23]

Researchers have put forward various PCF structures in recent years with good birefringence properties. A square-lattice fiber implementing square air holes with round corners was proposed by Ren et al.[24] This work achieved a high birefringence in the order of 10^{-3} but did not report on the EML of the design. Atakaramians et al.[25] investigated a rectangular air-hole porous fiber with a high birefringence value of 0.012 at 0.65 THz frequency. But this structure also exhibited an undesirably high EML of 25 cm^{-1} at the same frequency. Chen et al.[26] proposed a polymer porous fiber with elliptical air-holes and attempted to enhance the birefringence by rotating the major-axis of the air holes. A birefringence as high as 0.045 was obtained using this method. Li et al.[27] demonstrated a triangular lattice PCF with both circular and elliptical holes and achieved a birefringence up to 10^{-3} in the frequency range of 0.1 to 5 THz but with the drawback of having a high confinement loss. A dual-hole unit-based hexagonal PCF was proposed[28] in 2016 that yielded a birefringence of 0.033 but did not take into account the dispersion of the proposed waveguide. Later, Ahmed et al.[29] proposed a hexagonal cladding PCF with a high birefringence of 0.019 at 1 THz frequency. However, this work neglected to mention the confinement loss property of the proposed PCF. Recently, a slotted cladding PCF[30] and an oligoporous-core PCF[31] were shown to have high birefringence of 0.063 and 0.079, respectively. A slotted core design with uniquely shaped circular holes in the cladding by Monir et al.[32] achieved excellent birefringence and ultralow EML and confinement loss. The core in this work was formed by rectangular air slots surrounded by circular air holes. However, despite its superior results, it also has a massive drawback with respect to its dispersion properties. The dispersion values are in the 100's over the entire frequency range of 0.65 to 2 THz, which is around hundreds of times larger than our reported values. These results make this fiber undesirable for long distance transmission in comparison to our design. In addition, the large dispersion variation between ∼300 and −400 ps/THz/cm displayed by this fiber is highly unsuitable for simultaneous transmission of multiple signals in telecommunication applications.

In this paper, we propose and numerically analyze a novel PCF structure with a slotted core and Zeonex as the background material. The asymmetric core consists of rectangular air slots inside a hexagonal shape. The cladding is made asymmetric by incorporating a unique honeycomb-like structure with hexagonal air holes. This design is named as such since it resembles the honeycomb formation in a beehive. The air holes are placed in an intricate manner to minimize the amount of background material and enable the ease of fabrication. The asymmetry of the core and cladding results in ultrahigh birefringence, which is the main aim of this design. In addition, the proposed design also shows low EML and confinement loss, along with excellent dispersion characteristics in the frequency range of 1.4 to 2 THz. This PCF waveguide shows great potential for use in low-loss polarization-maintaining THz region applications.

2 Design Methodology

The cross-sectional view of the proposed PCF with honeycomb cladding is shown in Fig. 1, along with an enlarged view of the hexagonal core. The cladding consists of hexagonal air holes arranged in a honeycomb-like pattern. This design choice introduces a high level of asymmetry into the cladding, which facilitates ultrahigh birefringence. There are three rings of regular hexagonal air holes that follow an arithmetic sequence, with 12, 18, and 24 air holes in the first, second, and third ring, respectively. These air holes are equal in size and the distance between

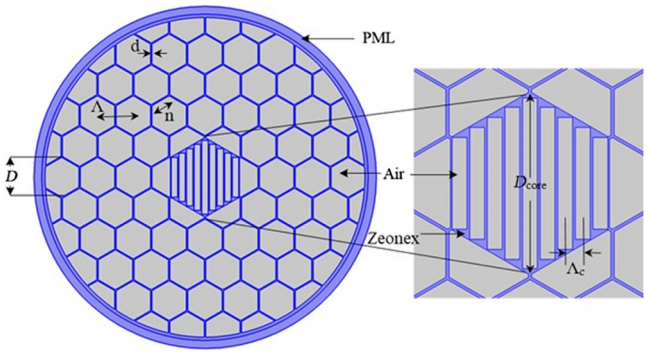

Fig. 1 Cross section of the proposed PCF with an enlarged view of the core.

opposite vertices of each hole is represented by D, with each side of the hexagons measuring $n = D/2$. The distance between the centers of adjacent air holes in the cladding, called the cladding pitch, is given by $\Lambda = 0.866D$ and is maintained at 180 μm. The strut width d, which is the distance between adjacent hexagonal air holes, is equal to 6.8 μm and is shown in Fig. 1. These distances are chosen in a manner so as to maximize the confinement of light within the core. The hexagonal slotted core consists of seven rectangular air slots with decreasing lengths away from the center of the core. The core diameter D_{core} has been varied in order to analyze its effects on the different guiding properties, and the variations of the core for different D_{core} values are displayed in Fig. 2. The lengths of the rectangular slots can be expressed in terms of the core diameter. The middle slot has length $0.93D_{\text{core}}$, its two adjacent slots are equal to $0.83D_{\text{core}}$, the two outermost slots have length $0.5D_{\text{core}}$ and the two remaining slots are $0.61D_{\text{core}}$ long. Although these lengths could be increased further to enhance birefringence, they are optimized in order to minimize difficulties in the fabrication process. In our investigation, we have also observed the effects of varying the porosity of the core, which is given by the ratio of the total area of rectangular air slots to the total area of the core. The porosity is varied by varying the width w of the rectangular slots while keeping the diameter of the core fixed. The center to center distance between adjacent rectangular slots is called the core pitch and is denoted by Λ_c.

For the background material of our proposed fiber, we have used Zeonex, the commercial name for Cyclo-olefin polymer. Zeonex provides a number of useful advantages over other materials, namely its low bulk material absorption loss of 0.2 cm^{-1} and the fact that it maintains a constant refractive index of $n = 1.525$ in the frequency range 0.1 to 1.5 THz.[33] In addition, it has very low material dispersion, is not affected by humidity and water vapor in the atmosphere due to having low hygroscopicity[30] and is highly suitable for biosensing applications.[31] A humidity insensitive fiber Bragg grating temperature sensor was fabricated by Woyessa et al.[34] with Zeonex as the cladding material. Utilizing the high glass transition temperature of Zeonex, the same author also characterized a Zeonex/PMMA-based microstructured polymer Bragg grating sensor for simultaneous monitoring of temperature and humidity,[35] and an endlessly single-mode polymer optical fiber temperature and strain sensor using Zeonex grade 480R.[36]

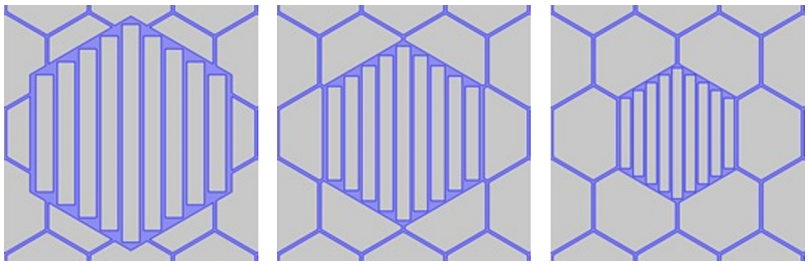

Fig. 2 Enlarged view of the core at different core diameters.

3 Results and Discussion

The commercially available COMSOL Multiphysics version 5.3 software based on the finite-element method has been used to design and simulate the proposed PCF waveguide. In order to accurately analyze the guiding properties of the fiber and calculate the losses, a circular perfectly matched layer (PML) boundary has been applied around the outside of the cladding. The PML acts as an antireflective layer[37] and absorbs electromagnetic waves propagating toward the cladding surface. The optimum thickness of the PML was determined by performing a convergence test, and it was found that a thickness of 5% of the total fiber radius shows the best results, which is the value we have chosen for this simulation. For the simulation, the bulk material absorption loss of Zeonex has been taken as 0.20 cm^{-1}, as mentioned previously. Since dry air is considered to be a completely transparent medium for waves in the THz range,[38] its absorption loss has been assumed to be zero for this investigation.

Figure 3 shows the mode field distributions of the proposed PCF for both x and y polarizations at different core porosities. It is clearly evident from this figure that the mode power is tightly confined within the porous core, which is essential for the transmission of THz waves. As the porosity is increased, the difference in refractive index between the core and the cladding reduces. As a result, the mode field starts to spread out toward the cladding region, which can be observed from this figure.

The variations of the effective refractive index of the proposed fiber with frequency and core diameter for both orthogonal polarization components at different core porosities are shown in Figs. 4 and 5, respectively. It can be seen from these figures that the effective index increases gradually both with increasing frequency and core diameter. At higher frequencies, some of the mode power starts to spread away from the core to the cladding, resulting in higher refractive index. When the core diameter is increased, the amount of solid Zeonex inside the core increases, which enhances the refractive index. The x polarization mode has higher effective index at all porosities compared to the y polarization mode, which indicates that light is more tightly confined inside the core for x polarization. Hence, we have chosen x polarization as the optimum mode for our design. The birefringence of a PCF is defined as the difference in refractive index of the x polarization and the y polarization mode and is mathematically given by

$$B = |n_x - n_y|, \tag{1}$$

where n_x is the refractive index of the x polarization mode and n_y is the refractive index of the y polarization mode. The birefringence as a function of frequency at different core porosities is shown in Fig. 6. It is observed that the birefringence increases very slowly with frequency up to 1.5 THz, and then remains almost flat from 1.5 to 2 THz. The increase occurs due to the enhancement of index contrast between the core and cladding at higher frequencies, which can also be seen from Fig. 4. On the other hand, the birefringence increases gradually with increasing D_{core}, which can be visualized from Fig. 7. When the core diameter is increased, the air slots become larger, which increases the asymmetry between the two polarization modes. Consequently, the index difference and thus the birefringence increases. From Figs. 6 and 7, it can be observed that the birefringence decreases with increase in core porosity. This is because at higher porosities, some of the mode power escapes from the slotted core into the cladding, reducing the refractive index difference between them. A birefringence value as high as 0.093 is obtained at 30% core

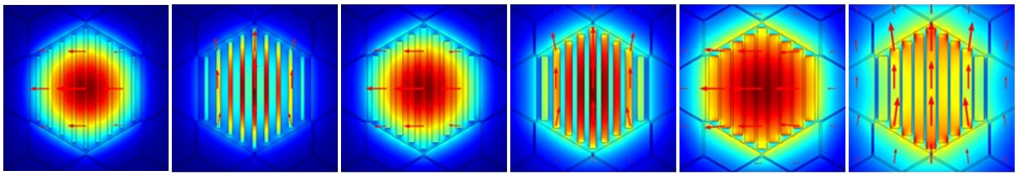

Fig. 3 Mode field profiles of the proposed fiber for (a), (b) x polarization and y polarization at 30% porosity; (c), (d) x polarization and y polarization at 50% porosity; and (e), (f) x polarization and y polarization at 70% porosity.

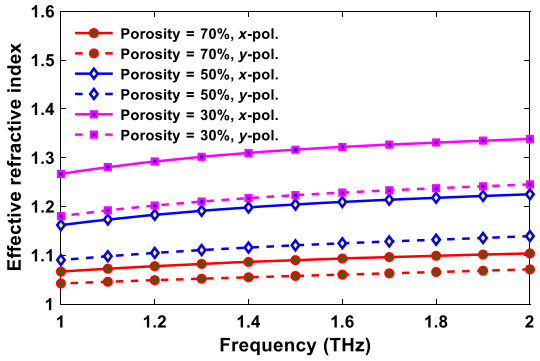

Fig. 4 Effective refractive index versus frequency of the fiber at different core porosities.

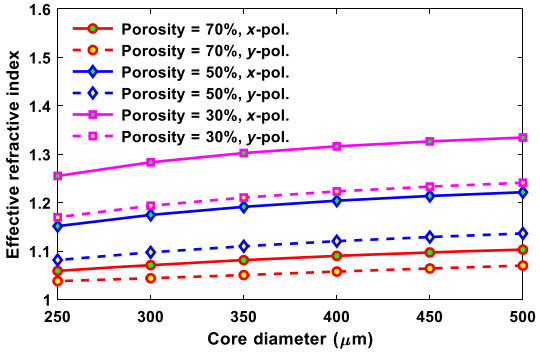

Fig. 5 Variation of effective refractive index with core diameter at different core porosities.

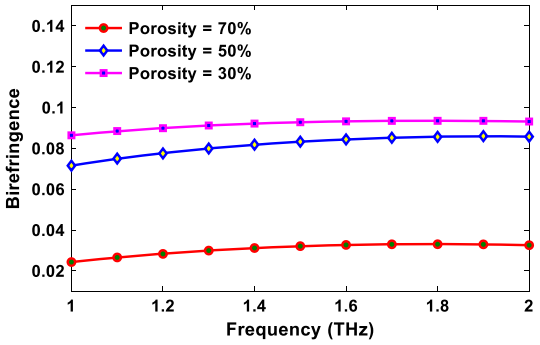

Fig. 6 Birefringence versus frequency of the fiber at different core porosities.

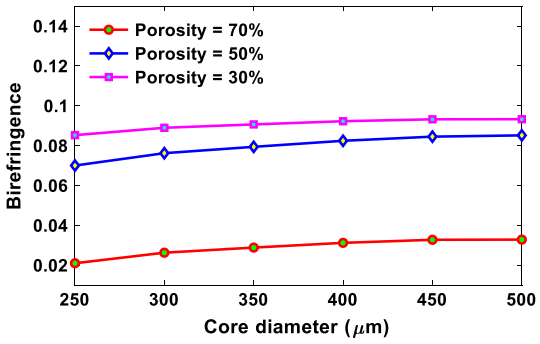

Fig. 7 Variation of birefringence with core diameter of the fiber at different core porosities.

porosity, $f = 2$ THz and $D_{\text{core}} = 500$ μm, which is one of the highest reported birefringences in the THz range to the best of our knowledge. However, in order to balance a high birefringence with lower losses, we choose 50% porosity, $f = 1.5$ THz and $D_{\text{core}} = 400$ μm as the optimum design parameters, which yields an ultrahigh birefringence of 0.083. Since birefringence is the most important property of a PCF waveguide for polarization maintaining applications, our proposed fiber shows excellent potential in this regard. It is very suitable for use in long-distance transmission and other applications requiring a high birefringence such as polarized filtering and optical sensing.

One of the biggest limiting factors in the propagation of THz waves along a PCF waveguide is the material absorption loss encountered by the waves due to the solid core material. This EML can be expressed by[39]

$$\alpha_{\text{eff}} = \sqrt{\frac{\epsilon_0}{\mu_0}}\left(\frac{\int_{\text{mat}} n_{\text{mat}}|E|^2\alpha_{\text{mat}}\text{d}A}{|\int_{\text{all}} S_z\text{d}A|}\right), \tag{2}$$

where α_{mat} and n_{mat} represent the bulk material absorption loss and the effective refractive index of Zeonex, respectively, ϵ_0 is the relative permittivity, μ_0 is the relative permeability of free space, and S_z is the z component of the Poynting vector given by, $S_z = 1/2 \times (E \times H*)z$, where E and $H*$ are the electric field component and complex conjugate of the magnetic field component, respectively. The integration in the numerator of Eq. (2) is performed only over the solid material, whereas the integration in the denominator is performed over the entire region. Figures 8 and 9 show the variation of EML of the fiber with frequency and core diameter, respectively, at different values of core porosity for the x polarization mode. EML increases gradually with both frequency[40] and core diameter, and increasing the core porosity results in lower EML. At higher core porosity, the amount of solid material is reduced and the mode power flows mostly through the rectangular air slots, resulting in lower EML. Conversely, increasing the

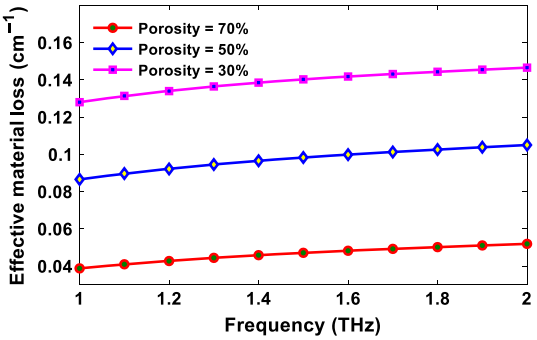

Fig. 8 Variation of EML with frequency of the proposed fiber at different core porosities for *x* polarization.

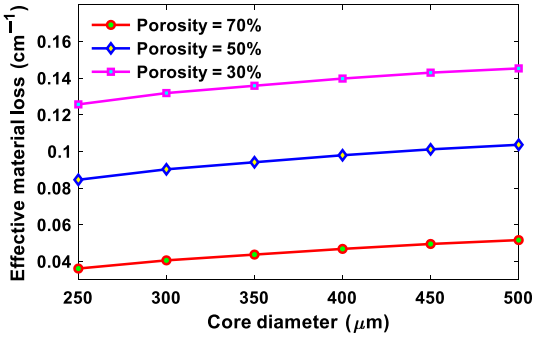

Fig. 9 Variation of EML with core diameter of the proposed fiber at different core porosities for *x* polarization.

core diameter causes the propagating electromagnetic field to encounter more of the solid material, which increases the EML. At the optimum design parameters of $f = 1.5$ THz, $D_{\text{core}} = 400\ \mu$m and 50% porosity, an extremely low EML of 0.095 cm^{-1} is obtained, which is comparable to the previously reported fibers in Refs. 28, 29, 31, and 41–46.

The core power fraction is defined as the amount of power that flows through the core air and represents how much useful power is propagating through the porous core. A high core power fraction is essential for obtaining ultrahigh birefringence and maintaining efficient transmission of THz waves.[47] It is given by the following equation:[48]

$$\eta' = \frac{\int_{\text{core}} S_z \mathrm{d}A}{\int_{\text{all}} S_z \mathrm{d}A'}, \tag{3}$$

where η' denotes the core power fraction. The region of interest in the numerator is the core area and the integration in the denominator is performed over the enter area of the fiber. The core power fraction of the x polarization mode as a function of frequency and core diameter is shown in Figs. 10 and 11. At 50% and 70% core porosity, the core power fraction increases with both frequency and core diameter but remains almost flat for 30% porosity. By increasing the core diameter, the total volume of air compared to the solid material in the core is increased, which increases the power fraction. At fixed diameter and frequency, the power fraction increases with core porosity. This can be explained by the fact that increasing the core porosity increases the amount of air inside the core, resulting in a higher amount of mode power flowing through the core air slots. However, it is observed that at very low frequencies of around 1 THz, the core power fraction is almost similar for 50% and 70% porosity. This is because, under low-frequency conditions, the confinement of light in the core is very low, and thus there is negligible difference between the core power fractions at these two porosities. Moreover, the core power fraction for 50% porosity is slightly higher than that for 70% porosity when the core diameter is very low.

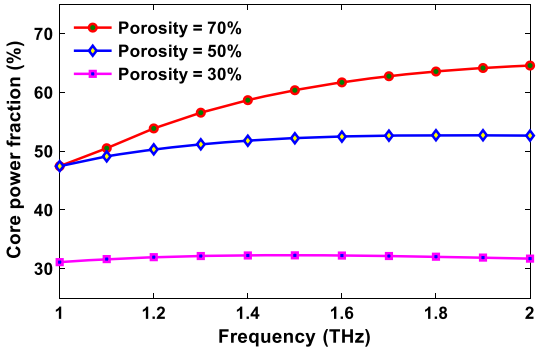

Fig. 10 Core power fraction versus frequency of the fiber at different core porosities for x polarization.

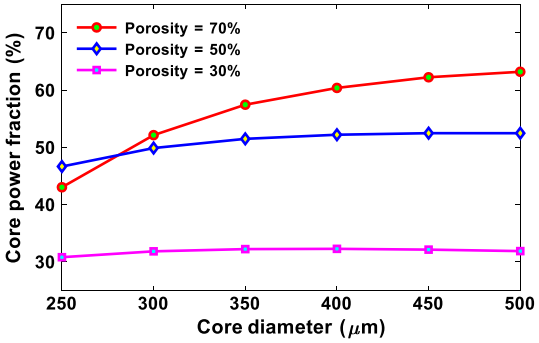

Fig. 11 Variation of core power fraction of the fiber with core diameter at different core porosities for x polarization.

This shows that when the core diameter is very small, it has a much greater effect on the core power fraction than the porosity. At the optimum design parameters of 50% porosity, $f = 1.5$ THz and $D_{\text{core}} = 400$ μm, a core power fraction of 52.2% is achieved, which ensures that the majority of the core power is concentrated within the air slots for efficient THz wave transmission. Although a higher porosity and core diameter could be used to enhance the power fraction, they also reduce the birefringence and increase the EML, respectively. Hence, our chosen parameters are retained.

In THz transmission, confinement loss is another important parameter to consider when designing a PCF. Confinement loss is defined as the amount of light that spreads out of the core into the cladding region and is mainly dependent on the lattice structure of the cladding. The confinement loss L_c is calculated from the imaginary part of the effective mode index by the following equation:[38]

$$L_c = \left(\frac{4\pi f}{c}\right)\text{Im}(n_{\text{eff}}), \tag{4}$$

where c is the velocity of light equal to 3×10^8 ms^{-1}, f is the frequency of operation, and $\text{Im}(n_{\text{eff}})$ is the imaginary component of the effective refractive index. Figure 12 shows that the confinement loss decreases steadily with increasing frequency for both x and y polarization modes. This is because, at higher frequencies, light is more tightly confined inside the slotted core region. The confinement loss for x polarization mode is observed to be lower compared to the y polarization mode since for x polarization mode, the index difference between the core and cladding is larger, which results in tighter confinement of light inside the core. Increasing the core porosity results in a corresponding increase in confinement loss. At high core porosity, there is a greater volume of air inside the porous core, which reduces the refractive index of the core. As a result, the index contrast between the cladding and the core is lower, and more light spreads out into the cladding region, which increases the confinement loss. At our chosen design parameters of $D_{\text{core}} = 400$ μm, $f = 1.5$ THz and 50% porosity, a good balance is maintained between the EML and confinement loss. Under these conditions, an ultralow confinement loss of around 10^{-8} cm^{-1} is achieved, which is almost negligible when compared with our obtained EML. This low value is made possible by the highly asymmetric honeycomb-like structure of the cladding.

Dispersion plays an important part in the long-distance transmission of THz waves since it indicates the extent to which spreading of pulses occur. In order to efficiently transmit signals over wide frequency ranges, the dispersion should be very small.[41] The dispersion should also show very little variation over wide ranges of frequency for simultaneous transmission of multiple signals. The induced material dispersion due to Zeonex is negligible since it has a constant refractive index in the range 0.1 to 1.5 THz. So we only need to consider the waveguide dispersion, which can be expressed by[49]

$$\beta_2 = \frac{2}{c}\frac{\text{d}n_{\text{eff}}}{\text{d}\omega} + \frac{\omega}{c}\frac{\text{d}^2 n_{\text{eff}}}{\text{d}\omega^2}, \tag{5}$$

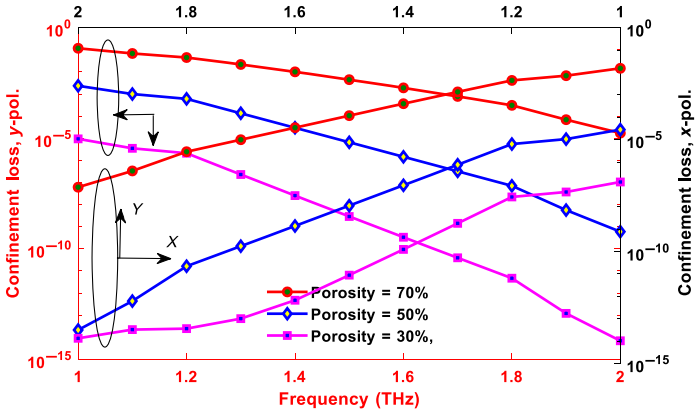

Fig. 12 Confinement loss versus frequency at different core porosities.

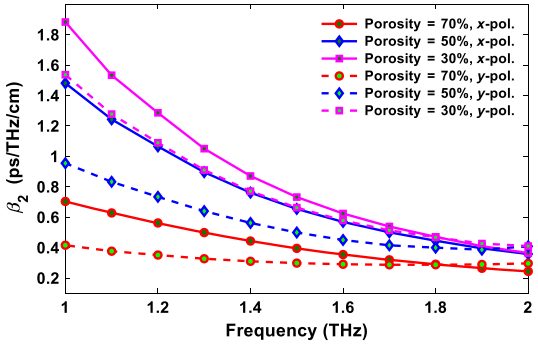

Fig. 13 Dispersion of the proposed PCF as a function of frequency for different core porosities.

where β_2 is the dispersion parameter, $\omega = 2\pi f$ indicates the angular frequency, c represents the speed of light in vacuum, and n_{eff} indicates the effective refractive index of the proposed PCF structure. The variation of dispersion with frequency of the fiber is demonstrated in Fig. 13 for both polarization modes at different core porosity values. It can be seen from this figure that at low porosities and low frequencies up to 1.4 THz, the dispersion variation for both x and y polarization modes is quite high. But from 1.4 to 2 THz, the proposed fiber displays flattened dispersion for both modes, which enables multiple signals to be transmitted simultaneously over this frequency range. Increasing the porosity causes the dispersion parameter to decrease in value and become more flat. For the x polarization mode, the dispersion is $\sim 0.56 \pm 0.20$ ps/THz/cm at the optimum design conditions.

We have considered two final parameters for our proposed fiber, which are the effective area and numerical aperture (NA). The effective area is given by the following relation:[50]

$$A_{\text{eff}} = \frac{\left[\int I(r) r \mathrm{d}r\right]^2}{\left[\int I^2(r) \mathrm{d}r\right]^2}, \tag{6}$$

where $I(r)$ is intensity distribution of the transverse electric field and is given by $I(r) = |E_t|^2$. On the other hand, the NA is given by the following equation:[51]

$$\text{NA} = \frac{1}{\sqrt{1 + \frac{\pi A_{\text{eff}} f^2}{c^2}}}. \tag{7}$$

The variation of both these parameters with frequency for the x polarization mode of the proposed fiber is shown in Fig. 14. It is observed that the effective area decreases steadily with increase in frequency. At higher frequencies, the mode field is strongly localized within the core air slots,[52] decreasing the effective area covered by the mode. In addition, increasing the porosity causes the effective area to increase. Since the index contrast between the cladding and the core is reduced with increasing porosity, the mode field starts to spread out from the core, which increases the effective area. At $f = 1.5$ THz, $D_{\text{core}} = 400$ μm and 50% porosity, a very high effective area of 0.9×10^{-7} m^2 is achieved for x polarization mode. From Fig. 14, we can observe that the NA decreases almost linearly with frequency and is higher at lower core porosity. At the optimum design conditions, the calculated NA is 0.36.

In order to implement our proposed fiber practically, we must consider whether its fabrication is possible using existing technologies. Numerous fabrication methods have been developed over the years, which include drilling,[53] stack and draw,[54] the sol–gel technique,[55] and among others. All these methods are suitable for fabricating microstructured circular air holes. However, our designed PCF has complex asymmetric structures in both the core and the cladding, with different shaped air holes. Kiang et al.[56] employed the extrusion technique for fabricating fibers with highly asymmetric structures. In addition, the 3-D printing method[57] has also been shown to be able to fabricate any complex PCF structure. Both of these methods are extremely feasible for

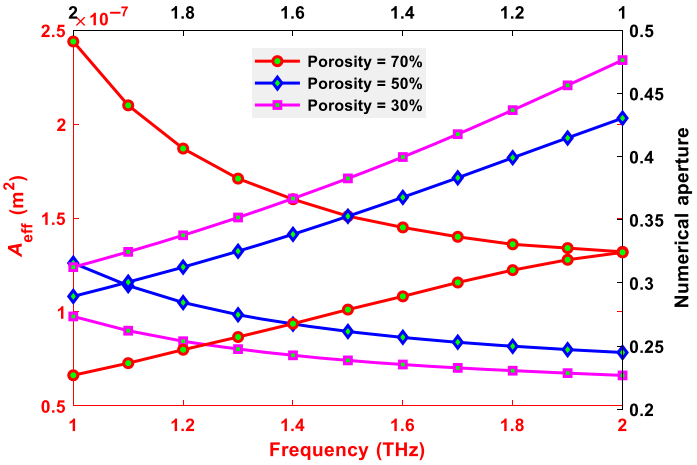

Fig. 14 NA and effective area as a function of frequency at different core porosities.

Table 1 Comparison of proposed fiber with some recently reported PCF.

Reference	Frequency (THz)	Birefringence (B)	Confinement loss (L_c)	Core PF (η') (%)	Dispersion B_2 (ps/THz/cm)
28	0.85	0.033	$>10^{-3}$ db/cm	32.5	—
29	1	0.0119	—	—	—
31	1	0.079	7.24×10^{-7} cm^{-1}	44	0.49 ± 0.05
32	1.1	0.24	6.5×10^{-12} dB/cm	—	—
41	1.5	0.08	—	48	0.7 ± 0.2
42	3	0.03	0.0004 cm^{-1}	58	0.2 to 1
43	1	0.0483	1.91×10^{-3} db/cm	37	0.51
44	1	0.0063	0.0036 cm^{-1}	46.9	0.53 ± 0.12
45	3	0.01	0.01 db/m	>40	0 to 1.5
46	1.2	0.051	7.2×10^{-3} db/cm	38	1.2 ± 0.32
Proposed PCF	1.5	0.083	10^{-8} cm^{-1}	52.2	0.56 ± 0.2

fabricating our proposed fiber. Furthermore, the similarly shaped hexagonal air holes in the cladding reduce the complexity of fabrication of both these techniques.

The characteristics of our proposed slotted core fiber are compared with some recently reported PCFs in Table 1. In addition to superior birefringence, our proposed PCF shows excellent characteristics, which make it highly suited for polarization-maintaining applications in the THz regime.

4 Conclusion

A slotted core PCF based on Zeonex is proposed and numerically analyzed. High asymmetry is introduced in the cladding using a novel honeycomb-like structure with three rings of hexagonal air holes. The various guiding properties of the proposed fiber are investigated with respect to frequency, core diameter, and core porosity. From the simulation results, an ultrahigh birefringence of 0.083 is obtained at 1.5 THz frequency, with minimal confinement loss and EML of 10^{-8} and 0.095 cm^{-1}, respectively. In addition, the proposed fiber shows nearly zero flattened

dispersion of 0.56 ± 0.2 ps/THz/cm in the frequency range 1.4 to 2 THz, along with a very high core power fraction of 52.2% and an effective area of 0.9×10^{-7} m^2 at the optimum design parameters. Practical implementation of the PCF structure using existing fabrication technologies has also been discussed thoroughly. The ultrahigh birefringence along with the excellent guiding properties makes the proposed fiber an excellent candidate for use in low-loss, polarization-preserving applications, and efficient transmission of THz waves.

References

1. M. Nagel et al., "Integrated THz technology for label-free genetic diagnostics," *Appl. Phys. Lett.* **80**(1), 154–156 (2002).
2. N. Laman et al., "7 GHz resolution waveguide THz spectroscopy of explosives related solids showing new features," *Opt. Express* **16**, 4094–4105 (2008).
3. J. B. Jensen et al., "Selective detection of antibodies in micro-structured polymer optical fibers," *Opt. Express* **13**(15), 5883–5889 (2005).
4. D. Pinto and S. S. A. Obayya, "Improved complex-envelope alternating direction-implicit finite-difference-time-domain method for photonic bandgap cavities," *J. Lightwave Technol.* **25**(1), 440–447 (2007).
5. H. Bolívar et al., "Label-free THz sensing of genetic sequences: towards 'THz biochips'," *Philos. Trans. R. Soc. London Ser. A* **362**(1815), 323–335 (2003).
6. M. Tonouchi, "Cutting-edge terahertz technology," *Nat. Photonics* **1**(2), 97–105 (2007).
7. W. Withayachumnankul et al., "T-ray sensing and imaging," *Proc. IEEE* **95**(8), 1528–1558 (2007).
8. R. H. Jacobsen, D. M. Mittleman, and M. C. Nuss, "Chemical recognition of gases and gas mixtures with terahertz waves," *Opt. Lett.* **21**(24), 2011–2013 (1996).
9. R. M. Woodward et al., "Terahertz pulsed imaging of skin cancer in the time and frequency domain," *J. Biol. Phys.* **29**(2), 257–259 (2003).
10. K. Wang and D. M. Mittleman, "Metal wires for terahertz wave guiding," *Nature* **432**(7015), 376–379 (2004).
11. H. Bao et al., "Dielectric tube waveguides with absorptive cladding for broadband, low-dispersion and low loss THz guiding," *Sci. Rep.* **5**, 7620 (2015).
12. H. Han et al., "Terahertz pulse propagation in a plastic photonic crystal fiber," *Appl. Phys. Lett.* **80**(15), 2634–2636 (2002).
13. M. Goto et al., "Teflon photonic crystal fiber as terahertz waveguide," *Jpn. J. Appl. Phys.* **43**(2B), L317 (2004).
14. K. Nielsen et al., "Bendable, low-loss Topas fibers for the terahertz frequency range," *Opt. Express* **17**(10), 8592–8601 (2009).
15. H. L. Bao et al., "Fabrication and characterization of porous-core honeycomb bandgap THz fibers," *Opt. Express* **20**, 29507–29517 (2012).
16. S. E. Kim et al., "Elliptical defected core photonic crystal fiber with high birefringence and negative flattened dispersion," *Opt. Express* **20**, 1385–1391 (2012).
17. A. Hassani, A. Dupuis, and M. Skorobogatiy, "Low loss porous terahertz fibers containing multiple subwavelength holes," *Appl. Phys. Lett.* **92**, 071101 (2008).
18. S. Atakaramians et al., "Porous fibers: a novel approach to low loss THz waveguides," *Opt. Express* **16**(12), 8845–8854 (2008).
19. R. Islam et al., "Novel porous fiber based on dual-asymmetry for low-loss polarization maintaining THz wave guidance," *Opt. Lett.* **41**(3), 440–443 (2016).
20. M. B. Byrne et al., "Simultaneous measurement of orthogonal components of polarization in a free-space propagating terahertz signal using electro-optic detection," *Appl. Phys. Lett.* **98**(15), 151104 (2011).
21. N. Karpowicz et al., "Coherent heterodyne time-domain spectrometry covering the entire 'terahertz gap'," *Appl. Phys. Lett.* **92**(1), 011131 (2008).
22. M. I. Hasan et al., "Design of hybrid photonic crystal fiber: polarization and dispersion properties," *Photonics Nanostruct. Fundam. Appl.* **12**(2), 205–211 (2014).
23. Y. Guo-Bing et al., "High birefringence, low loss terahertz photonic crystal fibres with zero dispersion at 0.3 THz," *Chin. Phys. B* **20**(9), 090701 (2011).

24. G. Ren et al., "Low-loss air-core polarization maintaining terahertz fiber," *Opt. Express* **16**, 13593–13598 (2008).
25. S. Atakaramians et al., "THz porous fibers: design, fabrication and experimental characterization," *Opt. Express* **17**(16), 14053–14062 (2009).
26. N.-N. Chen, J. Liang, and L.-Y. Ren, "High-birefringence, low-loss porous fiber for single-mode terahertz-wave guidance," *Appl. Opt.* **52**(21), 5297–5302 (2013).
27. S. Li et al., "Broadband high birefringence and low dispersion terahertz photonic crystal fiber," *J. Opt.* **16**, 105102 (2014).
28. G. K. M. Hasanuzzaman, S. Rana, and M. S. Habib, "A novel low loss, highly birefringent photonic crystal fiber in THz regime," *IEEE Photonics Technol. Lett.* **28**(8), 899–902 (2016).
29. K. Ahmed et al., "Ultrahigh birefringence, ultralow material loss porous core single-mode fiber for terahertz wave guidance," *Appl. Opt.* **56**(12), 3477–3483 (2017).
30. M. S. Islam et al., "Zeonex-based asymmetrical terahertz photonic crystal fiber for multichannel communication and polarization maintaining applications," *Appl. Opt.* **57**(4), 666–672 (2018).
31. M. S. Islam et al., "A novel Zeonex based oligoporous-core photonic crystal fiber for polarization preserving terahertz applications," *Opt. Commun.* **413**, 242–248 (2018).
32. M. K. Monir et al., "High birefringent, low loss and flattened dispersion asymmetric slotted core-based photonic crystal fiber in THz regime," *Int. J. Mod. Phys. B* **33**(20), 1950218 (2019).
33. J. Anthony et al., "Characterization of a microstructured Zeonex terahertz fiber," *J. Opt. Soc. Am. B* **28**(5), 1013–1018 (2011).
34. G. Woyessa et al., "Single mode step-index polymer optical fiber for humidity insensitive high temperature fiber Bragg grating sensors," *Opt. Express* **24**(2), 1253–1260 (2016).
35. G. Woyessa et al., "Zeonex-PMMA microstructured polymer optical FBGs for simultaneous humidity and temperature sensing," *Opt. Lett.* **42**(6), 1161–1164 (2017).
36. G. Woyessa et al., "Zeonex microstructured polymer optical fiber: fabrication friendly fibers for high temperature and humidity insensitive Bragg grating sensing," *Opt. Mater. Express* **7**(1), 286–295 (2017).
37. M. S. Islam et al., "Ultra low loss hybrid core porous fiber for broadband applications," *Appl. Opt.* **56**, 1232–1237 (2017).
38. J. Liang et al., "Broadband, low-loss, dispersion flattened porous-core photonic bandgap fiber for terahertz (THz) wave propagation," *Opt. Commun.* **295**, 257–261 (2013).
39. A. W. Snyder and J. D. Love, *Optical Waveguide Theory*, Chapman and Hall, New York (1983).
40. S. Rana et al., "Single-mode porous fiber for low-loss polarization maintaining terahertz transmission," *Opt. Eng.* **55**(7), 076114 (2016).
41. M. R. Hasan et al., "Polarization maintaining low-loss slotted core Kagome lattice THz fiber," *IEEE Photonics Technol. Lett.* **28**, 1751–1754 (2016).
42. Z. Wu et al., "Design of highly birefringent and low-loss oligoporous-core THz photonic crystal fiber with single circular air-hole unit," *IEEE Photonics J.* **8**(6), 4502711 (2016).
43. M. R. Hasan et al., "Polarization-maintaining low-loss porous-core spiral photonic crystal fiber for terahertz wave guidance," *Appl. Opt.* **55**(15), 4145–4152 (2016).
44. J. Luo et al., "Design and numerical analysis of a THz square porous-core photonic crystal fiber for low flattened dispersion, ultrahigh birefringence," *Appl. Opt.* **56**(24), 6993–7001 (2017).
45. Z. Wu et al., "Low-loss polarization-maintaining THz photonic crystal fiber with a triple-hole core," *Appl. Opt.* **56**(8), 2288–2293 (2017).
46. M. A. Habib and M. S. Anower, "Design and numerical analysis of highly birefringent single mode fiber in THz regime," *Opt. Fiber Technol.* **47**, 197–203 (2019).
47. L.-J. Chen et al., "Lowloss subwavelength plastic fiber for terahertz waveguiding," *Opt. Lett.* **31**(3), 308–310 (2006).
48. M. R. Hasan, M. A. Islam, and A. A. Rifat, "A single mode porous-core square lattice photonic crystal fiber for THz wave propagation," *J. Eur. Opt. Soc. Rapid Publ.* **12**, 15 (2016).

49. G. K. M. Hasanuzzaman et al., "Low loss single mode porous-core Kagome photonic crystal fiber for THz wave guidance," *J. Lightwave Technol.* **33**, 4027–4031 (2015).
50. R. Islam et al., "A novel low-loss diamond-core porous fiber for polarization maintaining terahertz transmission," *IEEE Photonics Technol. Lett.* **28**(14), 1537–1540 (2016).
51. S. Chowdhury et al., "Design of highly sensible porous shaped photonic crystal fiber with strong confinement field for optical sensing," *Optik* **142**, 541–549 (2017).
52. S. Roy, S. F. Kayser, and T. Azmaeen, "Design and optimization of a single mode octagonal photonic crystal fiber for high negative dispersion and high nonlinearity," in *5th Int. Conf. Inf., Electron. and Vision*, IEEE, pp. 614–619 (2016).
53. S. G. Johnson et al., "Linear waveguides in photonic-crystal slabs," *Phys. Rev. B* **62**(12), 8212–8222 (2000).
54. J. C. Knight, "Photonic crystal fibres," *Nature* **424**(6950), 847–851 (2003).
55. T. B. Ryan and T. Dennis, "Sol–gel-derived microstructured fibers: fabrication and characterization," in *Opt. Fiber Commun. Conf.*, Optical Society of America, paper OWL6 (2005).
56. K. M. Kiang et al., "Extruded singlemode non-silica glass holey optical fibres," *Electron. Lett.* **38**(12), 546–547 (2002).
57. H. Ebendorff-Heidepriem et al., "3D-printed extrusion dies: a versatile approach to optical material processing," *Opt. Mater. Express* **4**, 1494–1504 (2014).

Mohammad Rakibul Islam received his BScEngg and MScEngg degrees in electrical and electronic engineering from Bangladesh University of Engineering and Technology (BUET), Bangladesh, in 1998 and 2004, respectively, his MBA degree in marketing from the Institute of Business Administration (IBA) under the University of Dhaka in 2006, and his PhD from the Department of Electronics and Radio Engineering, Kyung Hee University, South Korea, in 2010. He joined the Department of Electrical and Electronic Engineering at Islamic University of Technology (IUT) as a faculty in 1999 and is serving as a professor there. He is currently the dean of Faculty of Science and Technical Education. His research interests include optical waveguide design, optical sensing, surface plasmon resonance, cooperative technique for wireless sensor networks, LDPC and QC-LDPC codes, secrecy capacity, and other wireless applications.

Md. Faiyaz Kabir received his BSc Eng degree in electrical and electronic engineering from Islamic University of Technology, Bangladesh, in 2017. He is currently working as a lecturer in the Department of Electrical and Electronic Engineering. His research interests include photonics, nanoplasmonics, silicon photonics, and fiber optics.

Khandoker Md. Abu Talha received his BSc degree in electrical and electronic engineering from IUT, Bangladesh, in 2018. Currently, he is working as a support engineer at Wipro Technologies Ltd. His research interests include optical sensing, photonic crystal fiber, biomedical sensing, surface plasmon, and supercontinuum generation.

Md. Shamsul Arefin received his bachelor's degree in electrical and electronic engineering from BUET in 2012, and is continuing his MSc degree at BUET currently. He did his thesis during BSc degree in biometric identification based on fingerprint recognition. He also published two IEEE conference papers in secrecy capacity for MIMO communication. He is currently working as a lecturer at Green University Bangladesh. His research interests include wireless communication, signal processing, wireless sensor networks, photonics, and their application in communication arena.